INDIAN JOURNAL OF SCIENCE AND TECHNOLOGY

RESEARCH ARTICLE

Benzene Sulfonamide Derivatives as Inhibitors for Steel Dissolution in Sulfuric Acid Solution

Amira E Ali[1], Ahmed Elmekabaty[1], Hanaa M Elabbasy[2], Mohamed F Atia[3], Gamila E Bad[1], Abd El-Aziz S Fouda[1]*

1 Chemistry Department, Faculty of Science, Mansoura University, Mansoura, 35516, Egypt
2 Misr Higher Institute for Engineering and Technology, Mansoura, Egypt
3 Chemistry Department, Faculty of Science, Tanta University, Tanta, Egypt

OPEN ACCESS

Received: 05-02-2023
Accepted: 01-08-2023
Published: 30-09-2023

Citation: Ali AE, Elmekabaty A, Elabbasy HM, Atia MF, Bad GE, Fouda AEAS (2023) Benzene Sulfonamide Derivatives as Inhibitors for Steel Dissolution in Sulfuric Acid Solution. Indian Journal of Science and Technology 16(37): 3073-3089. https://doi.org/10.17485/IJST/v16i37.259

* **Corresponding author**.

asfouda@hotmail.com

Funding: None

Competing Interests: None

Published By Indian Society for Education and Environment (iSee)

ISSN
Print: 0974-6846
Electronic: 0974-5645

Abstract

Objectives: To examine the effectiveness of various benzene sulfonamide derivatives in preventing the corrosion of carbon steel in H_2SO_4 and to identify the dominating active form of the used compounds throughout the adsorption process in order to better understand the mechanism of their action. **Methods:** N-(4-(2-Aminothiazol-4-yl) phenyl) benzene sulfonamide (A) and N-(4-(2-thioxo-1, 2-dihydropyrimidim—4-yl) phenyl) benzene sulfonamide (B) were the tested compounds and were chosen based on molecular structure. To examine the effectiveness and mechanism of inhibition, the mass method (ML) has been combined with a number of electrochemical methods, including potentiodynamic polarization (PP) and electrochemical impedance spectroscopy (EIS). Fourier-transform infrared spectroscopy (FT-IR), scanning electron microscopy (SEM), energy dispersive X-ray spectroscopy (EDX), and atomic force microscope (AFM) techniques also, were used to confirm the adsorption phenomenon. **Findings:** The concentration and chemical makeup of the examined benzene sulfonamide derivatives greatly influence their ability to inhibit. These substances have mixed-type inhibitory properties and work by adhering to surfaces in accordance with the Temkin adsorption isotherm. The investigated benzene sulfonamide derivatives' ability to inhibit might be related to their physisorption on the metal surface, which occurs when the inhibitors' protonated form interacts with the charged metal surface. **Novelty:** This paper provides useful information regarding inhibition effect of benzene sulfonamide derivatives. The outcome of this work contributes to better understanding of the mechanism of inhibition by quantum chemical examination and Monte Carlo model and to provide more information on carbon steel corrosion for academic and starting researchers.

Keywords: Corrosion inhibition; Carbon steel; H_2SO_4; Sulfonamide derivatives; FTIR; SEM; EDX; AFM

1 Introduction

Metal dissolution is a serious problem which can be reduced, but cannot be completely prevented. One of the most popular, efficient, and cost-effective ways to protect metals in an acidic environment is to use corrosion inhibitors to prevent corrosion [1]. The majority of well-known acid corrosion inhibitors are organic compounds with N, S, or O atoms [2] that can adsorb on the surface of the metal. While many of these chemicals are harmful by nature, nontoxic or significantly less toxic versions have been developed. Benzene sulfonamide molecules are one of these substances. These substances are part of a crucial class of substances with a wide range of applications. These substances have shown to be effective corrosion inhibitors. According to reports, they have no environmental impact at the concentrations seen in corrosion inhibitors [3]. Carbon steel is extremely strong and impact resistant [4]. This makes it a popular choice for modern road construction, pipe and support. Like tubes, carbon steel can be very thin compared to other metals [5]. Therefore, carbon steel is used in the petroleum industries such as acids which corrode metals, as it removes the oxide layer from its surface, increasing the corrosion process [6]. According to a survey of the literature, the employ of organic chemicals as inhibitors of CS corrosion in acidic environments has been known for quite some time [4,6]. Mostafa et al. [7] synthesized azopyrazole-benzenesulfonamide derivative and used it as an efficient corrosion inhibitor for mild steel in acidic environment. Novel hydrazide derivatives were used as corrosion inhibitors for mild steel in HCl solution by Farag et. al [8]. Thiosemicarbazide derivative was utilized as Anticorrosion inhibitor for mild steel in 0.5 M sulfuric Acid solution [9].

As a result, utilizing ML and electrochemical techniques, the current research describes a study of the corrosion protective activity of certain sulfonamide derivatives on CS corrosion in solutions of o.5 M sulfuric acid. Efficacy of inhibition at altered doses of inhibitors in acidic media was investigated and discussed. Temperature effects on CS dissolving in free acids and inhibited acids solutions were also investigated.

2 Methodology

2.1 Material and solutions

Chemical composition of CS was as follows**:** C 0.61%, Mn 0.724%, P 0.013% S 0.254% and Fe balance. Corrosive media (Sulfuric acid): The appropriate volume of pure reagent (98%) was diluted by bi-distilled water and titration was utilized to determine the acid's concentration. Inhibitors as below:

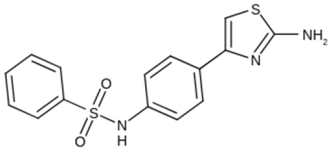

Fig 1. N-(4-(2-Aminothiazol-4-yl) phenyl) benzene sulfonamide; Mol. Wt.=331.41; Mol. Formula = $C_{15}H_{13}N_3O_2S_2$

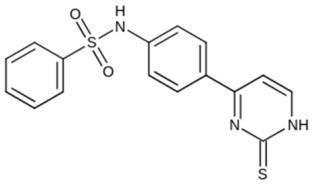

Fig 2. N-(4-(2-thioxo-1, 2-dihydropyrimidim–4-yl) phenyl) benzene sulfonamide; Mol. Wt. = 343.04; Mol. Formula = $C_{16}H_{13}N_3O_2S_2$

In order to create the stock solutions (10^{-3} M) of the chemicals, ethanol (99%) and DMF were used as organic solvents. By dilution the chemicals with bi-distilled water, the used concentrations (10 x10^{-6} to 50 x10^{-6} M) were created.

2.2 Chemical methods

We divided the carbon steel into 6 equal parts (20 x 20 x 2 mm). Emery paper is used to mechanically abrade the CS specimen, and acetone is used to degrease it before being cleaned through bi-distilled water and dried utilizing filter papers before the investigations begin. The components are weighed after sanding and drying. Glass hooks are employed to ensure that the whole surface of the CS samples is submerged in the corrosive solution and uniformly attacked.[10] The initial portion is submerged in 0.5 M H_2SO_4. The remaining fragments are submerged in inhibited acidic solutions with different chemical concentrations (10 $x10^{-6}$ to 50 $x10^{-6}$ M). The components are weighed after appointed time. Three hours are spent on the experiment and repeating this experiment at various temperatures from (25 to 45°C).

$$\%IE = [1 - (\Delta Winh / \Delta W free)] x100 = \theta x100" \quad (1)$$

$$CR = \Delta W \setminus at" \quad (2)$$

Since "ΔW_{inh} and ΔW_{free}" are, respectively, the corresponding loss in the mass in substance under investigation and absence, "%IE" is efficacy of inhibition of the substance under investigation, "C.R" is rate of deterioration of CS, and "a and t" are CS area and time spent immersed, respectively.

2.3 Non-chemical technique

Through the use of the Gamry Framework TM and the Gamry Potentiostat G-750, these procedures were performed three times. Two separate electrochemical techniques were used to assess CS's susceptibility to corrosion in 100 ml of half-molar H_2SO_4 with and without the researched inhibitors. All of these procedures were conducted in a 25°C electrochemical glass cell has three electrode systems. As the working electrode, a 1 cm^2 CS specimen is used. The auxiliary electrode is platinum, and the reference electrode is saturated calomel electrode (SCE). To produce the CS electrode, a CS specimen is joined via welding from one side and skillfully encased within glass rod, leaving only one direction of CS exposed to the employed corrosive medium. The CS electrode is cleaned in accordance with the ML procedure. Gamry Instrument (PCI4/750) with computerized outlines operated electrochemical procedures with DC105 software for PP experiments additional to EIS300 programmer for electrochemical impedance (ac) spectroscopy methods. For fitting, graphing, and displaying the acquired data. "To obtain the PP data, the electrode potential was automatically shifted from -1000 to 0 mV vs. SCE at a scan rate of 0.2 mV s^{-1}.EIS was done using ac signals at open circuit potential in the frequency range of 100 kHz to 0.1 Hz with amplitudes of 10 mV peak-to-peak.[11]

2.4 Surface examination techniques

For all surface examination tests, the CS specimens were prepared as described in ML method before dipping for 24 hours in half molar H_2SO_4 without and with $50x10^{-6}$ M at 25°C.

2.4.1 ***Fourier-transform infrared spectroscopy (FT-IR) analysis***

Using an FT-IR spectrophotometer that produces an infrared spectrum "(Model 960 Mooog, ATI Mattson Infinity Series, USA)", the function groups of the inhibitor derivatives were examined.

2.4.2 ***Scanning electron microscopy (SEM) analysis***

This technique gives a photograph of CS before and after immersion. SEM model A Jeol JSM-5400 instrument was used in the investigation.

2.4.3 ***Energy dispersive X-ray (EDX) analysis***

This EDX examination was employed to compare the components on the CS surface prior to and following dipped into the inhibitor solution.

2.4.5 ***Quantum calculations***

Using Material Studio version 6's semi-empirical approach (PM3), the entire quantum chemistry study has been conducted. Semi-empirical methodology was used to calculate molecular orbitals. This technique was employed with comprehensive geometry optimization.

3 Results and Discussion

3.1 M L Method

Figure 3 shows mass loss-time curves at which CS dissolves in a half molar of H_2SO_4 with the exist and non-exist of various dosages of chemical (A) and chemical (B). The ML of CS in the occurrence of the chemicals has substantially lower than the blank solution and changes linearly with time. The CS dissolution a half molar of H_2SO_4 is accompanied by the generation of soluble corrosion products, according to the linear fitting of the ML-time relation. The examined chemicals' adsorption onto the metal surface is what causes the inhibition.

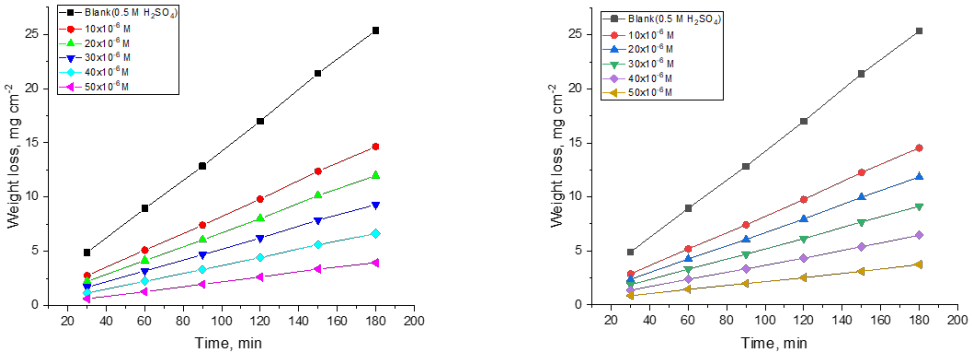

Fig 3. ML-time curves for CS dissolving in a half molar of H_2SO_4 with the exist and non-exist of various dosages of the investigated compounds at 25 °C

3.2 Temperature impact

Variation of efficacy of inhibition (% IE) of derivatives (A& B) with temperature were dedicated in Tables 1 and 2, respectively. From these Tables, it was found that, there's an inverse relationship between temperature and inhibition, indicating inhibitors physisorption to CS surface.[12]

Table 1. % IE of compound (A) from ML tests at 2hrs dispersion in a half molar H_2SO_4 at different temperatures from (25-45 °C)

Conc., M	Temp., ° C	k_{corr} mg cm^{-2}min^{-1}	Θ	%IE
	25	0.024±0.0012	0.831	83.1
	30	0.043±0.0018	0.828	82.8
10 x10^{-6}	35	0.056±0.0009	0.796	79.6
	40	0.081±0.0011	0.779	77.9
	45	0.107±0.0020	0.776	77.6
	25	0.024±0.0015	0.839	83.9
	30	0.039±0.0014	0.834	83.4
20 x10^{-6}	35	0.054±0.0011	0.8	80
	40	0.081±0.0017	0.787	78.7
	45	0.107±0.0018	0.783	78.3
	25	0.023±0.0018	0.84	84
	30	0.037±0.0021	0.835	83.5
30 x10^{-6}	35	0.052±0.0014	0.803	80.3
	40	0.079±0.0020	0.795	79.5
	45	0.098±0.0012	0.794	79.4
	25	0.022±0.0012	0.855	85.5
	30	0.036±0.0012	0.843	84.3
40 x10^{-6}	35	0.051±0.0021	0.806	80.6
	40	0.074±0.0012	0.795	79.5

Continued on next page

Table 1 continued

	45	0.098±0.0035	0.794	79.4
	25	0.021±0.0009	0.855	85.5
	30	0.036±0.0018	0.852	85.2
50 x10^{-6}	35	0.050±0.0012	0.813	81.3
	40	0.073±0.0014	0.806	80.6
	45	0.097±0.0021	0.795	79.5

Table 2. %IE of compound (B) from ML tests at 2hrs dispersion in a half molar H_2SO_4 at different temperatures from (25-45 °C)

Conc., M	Temp., ° C	k_{corr} mg cm^{-2} min^{-1}	Θ	%IE
	25	0.028±0.0014	0.827	82.7
	30	0.044±0.0020	0.807	80.7
10 x 10^{-6}	35	0.050±0.0014	0.806	80.6
	40	0.083±0.0014	0.793	79.3
	45	0.104±0.0882	0.772	77.2
	25	0.027±0.0017	0.833	83.3
	30	0.044±0.0012	0.823	82.3
20 x10^{-6}	35	0.048±0.0012	0.811	81.1
	40	0.080±0.0014	0.806	80.6
	45	0.011±0.0012	0.786	78.6
	25	0.024±0.0017	0.842	84.2
	30	0.037±0.0014	0.836	83.6
30 x10^{-6}	35	0.042±0.0026	0.824	82.4
	40	0.076±0.0017	0.814	81.4
	45	0.100±0.0100	0.789	78.9
	25	0.022±0.0018	0.851	85.1
	30	0.028±0.0012	0.844	84.4
40 x10^{-6}	35	0.039±0.0017	0.825	82.5
	40	0.075±0.0020	0.816	81.6
	45	0.098±0.0012	0.79	79
	25	0.021±0.0015	0.865	86.5
	30	0.026±0.0021	0.853	85.3
50 x10^{-6}	35	0.037±0.0011	0.845	84.5
	40	0.067±0.0021	0.832	83.2
	45	0.091±0.0014	0.796	79.6

3.3 Thermodynamic corrosion parameters

It is evident that the CS dissolving rate rises with rising solution temperature and follows Arrhenius type equation in both the non-existence and existence of the studied derivatives.[13,14]. The activation energy (E_a^*) value was determined by employing an Arrhenius-type Eq. **(Figure 4),** that it was as follows:

$$"kcorr = A\ exp\ (-Ea*/RT)" \tag{3}$$

Since "k_{corr}" is rate of CS corrosion, "R and T" are, respectively, gas constant and Kelvin temperature. The transition-state Eq. **(Figure 5)** was used to attain the enthalpy (ΔH^*) and entropy (ΔS^*) data of activation that it was as follows:

$$"kcorr/T = (R/Nh)\ exp\ ((\Delta S*/R)\ exp\ -\ (\Delta H*/RT)]" \tag{4}$$

Table 3 Illustrates the measured activation parameters. From Table 3, one noticed that:

1. Adsorption of the chemicals on CS surface is physically because of the magnitude of apparent E_a^* increases in the existence of investigated derivatives than in their nonexistence, because at higher temperatures, the average kinetic energy of extract components rises, making the adsorption between extract components and a metal surface insufficient to keep the species at the binding site and potentially leading to desorption or causing the species to bounce off the surface of the metal instead of colliding and combining with it.[15] Furthermore, since the protective layers on the metal surface would have been more soluble at a higher temperature, the metal surface would have been exposed to the hostile medium and would have experienced more disintegration, additional to enthalpy of activation (ΔH^* below 100 kJ mol^{-1}).

2. "The exothermic nature is shown by the negative sign of (ΔH^*)".
3. The dissolution process may involve H_2 evolution reaction, due to all of E_a^* values of are above than ΔH^* values.
4. The ΔS^* positive sign denotes the increase of disorder in the formation of activated state. [15]

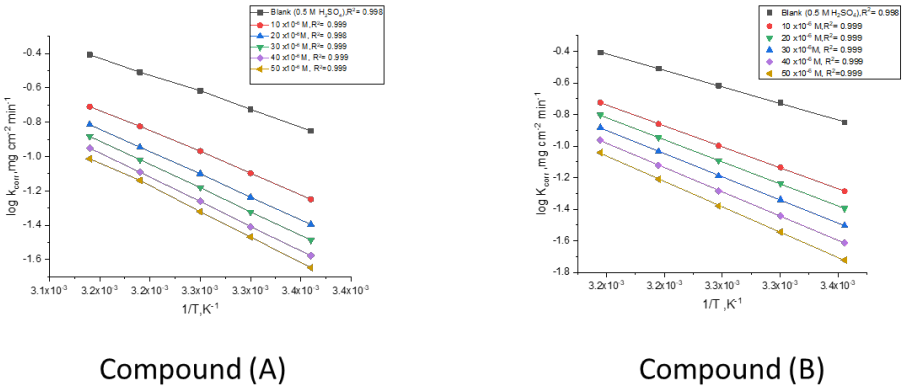

Fig 4. log k_{corr} vs. 1/T curves for CS in a half molar of H_2SO_4 with and without various dosages of the investigated compounds

Table 3. CS activation parameters in a half molar of sulfuric acid with and absence of various dosages of organic derivatives

Compound	Inh., Mx10^6	E^*_a, kJ mol^{-1}	-ΔH^*, kJ mol^{-1}	-ΔS^*, J mol^{-1}K^{-1}
Blank	**o.5M H_2SO_4**	39.7±0.0882	37.1±0.2027	199.1±0.173205
	10	57.2±0.1732	52.4±0.2333	179.0±0.115470
	20	58.2±0.2333	53.4±0.1155	164.3±0.08819
A	30	58.5±0.2309	53.7±0.1202	154.3±0.08819
	40	58.6±0.0882	54.0±0.0882	141.5±0.230940
	50	59.6±0.2333	54.7±0.1764	137.7±0.08819
	10	51.5±0.1453	49.2±0.1527	180.4±0.173205
	20	52.8±0.0577	51.4±0.1202	154.4±0.176383
B	30	57±0.1202	52.6±0.1764	137.6±0.08819
	40	60.9±0.1202	57.7±0.1333	126.2±0.152752
	50	62.5±0.2309	60.9±0.1453	120.3±0.176383

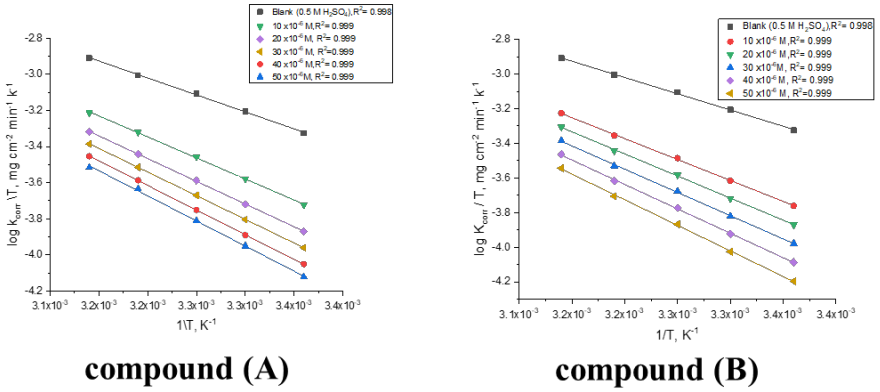

Fig 5. log k_{corr}/T vs. 1/T curves for CS in a half molar of H_2SO_4 with and without various dosages of the investigated compounds

3.4 Adsorption isotherms

"It is evident that the examined derivatives adhere to the Temkin isotherm during their adsorption on the surface of metal"

$$"\theta coverage \ = \ (2.303a) \ [Log \ Kads \ + Log \ C]" \tag{5}$$

A plot of surface coverage ($\Theta_{coverage}$) and derivatives concentration (Log C) results in straight lines **(Figure 6)** indicating that the adsorption of the derivatives on the surface of CS is consistent with Temkin isotherm with the correlation coefficient (R^2) close to unity. From intercept, we calculate standard desorption constant K_{ads} which denotes the strength between the adsorbate and the adsorbent. Employing the following Eq., the standard free energy (ΔG°_{ads}) data for adsorption can be attained.

$$Kads \ = \ "(1\backslash 55.5) \ exp \ (- \Delta G^{\circ} ads \ \backslash RT)" \tag{6}$$

Using the fundamental Van't Hoff's Eq. , a straight line emerges from drawing log K_{ads} vs. (1/ T) **(Figure 7)**. ΔH°_{ads} were obtained from the slope:

$$"Log \ Kads = \ (- \Delta H^{\circ} ads / \ 2.303RT) \ + \ constant" \tag{7}$$

By introduction the obtained ΔG°_{ads} and $\Delta H^{\circ}_{ads,}$ the entropy (ΔS°_{ads}) data of adsorption was determined at all studied temperature.

$$"\Delta Goads = \ \Delta H^{\circ} ads \ - \ T\Delta S^{\circ} ads \ " \tag{8}$$

The determined values of adsorption parameters were introduced in Table 4. From this Table, it was noticed that:

1. The K_{ads} data demonstrated that the adsorption coefficient reduces as temperature rises. Given that K_{ads} was higher at 298 K than it was at 318 K, it is likely that a greater amount of the derivatives were adsorbed onto the surface of the CS. This suggests that lower temperatures are advantageous for the inhibition process.
2. The negative ΔG°_{ads} data demonstrates both the "spontaneity of the process and the settlement of the adsorbed layer.[16]
3. Values of ΔG^{o}_{ads} lower than -20 kJ mol^{-1} are consistent with the electrostatic interaction between the charged molecules and the charged metal (physical adsorption).[16] The values of ΔG^{o}_{ads} for utilized derivatives are between 18-19.2 kJ mol^{-1} indicate physical adsorption.
4. "The negative sign of ΔH°_{ads} indicates that the adsorption of derivative molecules is an exothermic, this means that the adsorption process may be physical or chemical.
5. Because the ΔH°_{ads} data are low less than 80 kJ mol^{-1} the investigated chemicals are physically adsorbed onto the CS surface.

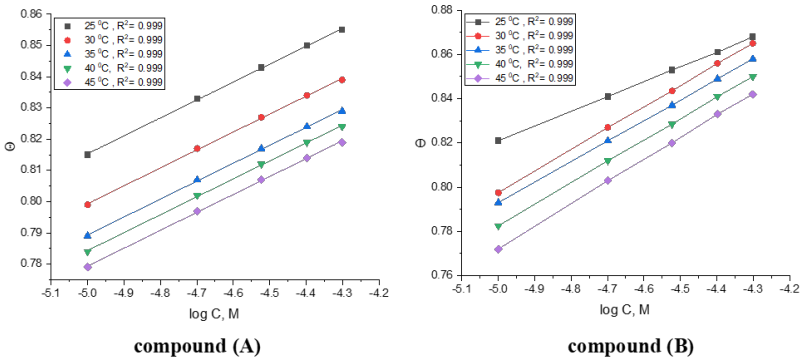

Fig 6. Plots of Temkin isotherm for compounds (A) and (B) on CS at different temperatures in half molar H_2SO_4

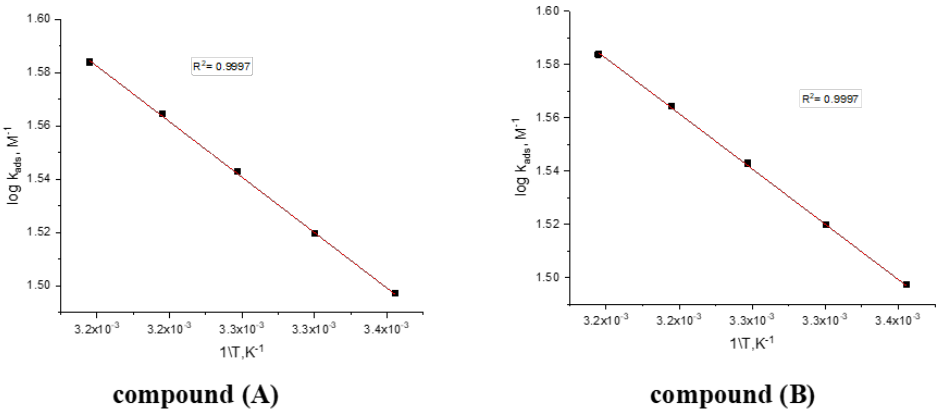

Fig 7. (1/ T against log K_{ads}) with and without various concentrations of compounds (A) and (B)

Table 4. Thermodynamic adsorption parameters data

Inhibitor	Temp. K	$K_{ads}M^{-1}$	$-\Delta G^{\circ}_{ads,}$kJ mol^{-1}	$-\Delta H^{\circ}_{ads}$kJ mol^{-1}	$-\Delta S^{\circ}_{ads}$J mol$^{-1}K^{-1}$
	298	41.4	19.2		37.9
	303	32.0	18.8		35.9
A	308	31.7	19.1	7.9	36.3
	313	29.4	19.3		36.4
	318	27.4	19.4		36.2
	298	29.6	18.3		36.2
	303	22.2	18.0		34.6
B	308	21.3	18.1	7.5	34.4
	313	21.2	18.4		34.8
	318	17.4	18.2		33.6

3.5 Non-chemical technique

3.5.1 ***EIS method***

Nyquist and Bode plots for CS degradation in H_2SO_4 (half molar) with and without examined derivatives at 25°C are represented in Figures 8 and 9. The EIS diagram exhibits a nearly single semi-circuit, demonstrating that the metallic dissolution phase is accompanied by a single charge transfer mechanism that is unaffected by the presence of examined chemicals[17]. Small distortion was found owing to electrode roughness, contaminants, and inhibitor adsorption, which resulted in the creation of porous layers and a uniform electrode surface[18]. "The analogous circuit shown in Figure 10 is utilized to study the impedance spectra. R_s is the solution resistance between the CS electrode and the reference electrode in this circuit", whereas CPE denotes the charge phase element. The accuracy of the fitted data is also assessed using the chi-squared (χ^2). Table 5 shows that the "χ^2" values are low indicating that the fitted data and the experimental data concur well. A double layer's capacity (C_{dl}) is given as follows:

$$"Cdl = Yo\,(\omega max)^{n-1}" \tag{9}$$

Since "n, ω, and Yo" are, respectively, CPE exponent, maximum frequency and CPE coefficient. The %IE and (θ) of the studied chemicals were gained from EIS measurements as follows:

$$"\%IE = [(Rct - Roct)\backslash Rct]\,x\,100 = \theta\,x100" \tag{10}$$

Since "R_{ct} & R^{o}_{ct}" are, respectively, a charge transfer resistances in the existence of the chemicals being investigated and absent. Radius of Nyquist diagrams growths with raising the concentration of the investigated derivatives as a result of forming chemicals' adsorbed layer onto CS. According to Table 5 (EIS parameters for CS corrosion), we conclude that:

1. A slower corroding system is linked to a high charge transfer resistance (R_{ct}). R_{ct} (derivative B) > R_{ct} (derivative A) at any given inhibitor dose, indicating that derivative (B) has superior inhibitory effectiveness to derivative (A). The derivative (B) has a S atom connected to a heterocyclic ring in its structure, which increases the electronic cloudiness on the molecules and, as a result, improves the derivative (B) capacity's for adsorption on the CS surface.
2. The fact that C_{dl} values drop as the concentration of the examined derivatives is increased and that this is due to the replacement of water molecules in the double layer by adsorbed inhibitors. "This was caused by a drop in the local dielectric constant or an increase in the thickness of the electrical double layer". "This indicates that the inhibitor molecules work by adsorption at the metal/solution interface".

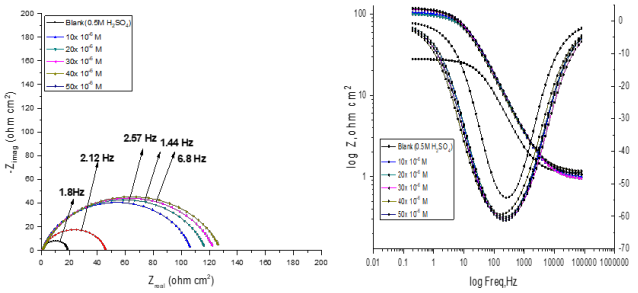

Fig 8. Nyquist and Bode curves for CS in a half molar of H_2SO_4 with and without various dosages of chemical (A) at 25°C

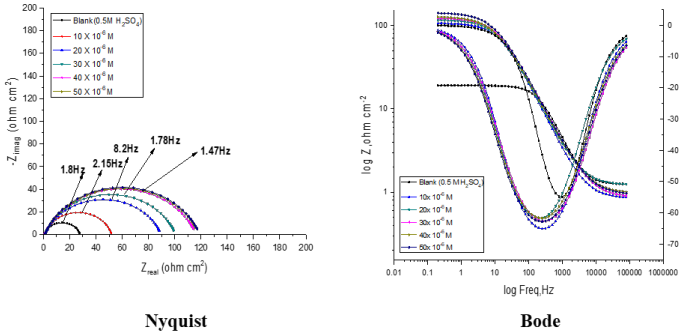

Fig 9. Nyquist and Bode for CS in a half molar of H_2SO_4 with and without various dosages of chemical (B) at 25 °C

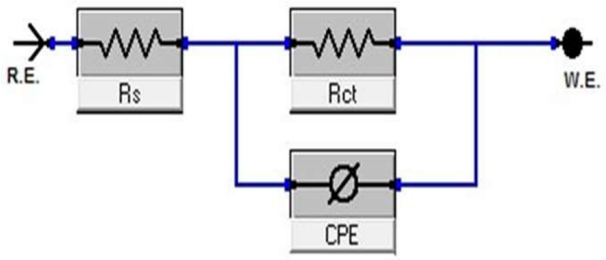

Fig 10. Circuit employed for matching EIS data

Table 5. EIS outcomes for CS corrosion in exist and non-exist of altered doses of organic derivatives at 25°C

Compound	[Inh]M x 10^{-6}	$R_{ct}\Omega$ cm^{-2}	$C_{dl}\mu F$ cm^{-2}	$\chi^2 x10^3$	Θ	%IE
Blank	**0.5M H_2SO_4**	10.36±0.2021	206.3±0.1453	1.121	–	–
	10	93.50±0.1453	71.2±0.1732	4.342	0.889	88.9
	20	93.76±0.2318	70.0±0.0667	6.121	0.890	89.0
A	30	100.5±0.1453	69.3±0.1154	5.111	0.897	89.7
	40	125.4±0.1764	54.5±0.2027	4.551	0.917	91.7
	50	128±0.2082	54.0±0.1453	5.323	0.919	91.9
	10	81.4±0.1732	85.9±0.1732	4.413	0.873	87.3
	20	91.50±0.1453	71.4±0.1155	7.123	0.887	88.7
B	30	102±0.1764	68.8±0.088	6.332	0.898	89.8
	40	119±0.1202	54.8±0.2603	5.342	0.913	91.3
	50	131.4±0.2333	50.7±0.1155	4.456	0.921	92.1

3.6 PP technique

Tafel plots **(Figure 11)** were employed for description of corrosion mechanism of CS in half molar H_2SO_4. "The current density of the anodic and cathodic branch is moved towards lower values" by examination of the polarization curves following the addition of derivatives (B) and (A), and the displacement is more pronounced with an increase in inhibitor concentration indicating that the derivatives are mixed-type. [19]. The IE is estimated from the next Eq.:

$$"\%\ IE\ =\ [(ifree\ -\ iinh)\ /\ ifree]\ x\ 100" \tag{11}$$

with "i_{free} and i_{inh}" as corrosion current density in non-exist and exist chemicals, respectively. By extrapolating the current-potential lines to the relevant corrosion potentials, corrosion current densities were calculated. In this case, the corrosion rates were computed under the presumption that corrosion is attacking the entire steel surface and that local corrosion is not present. From Table 6 (PP parameters for CS corrosion), it was found that:

1. The current density of corrosion (i_{corr}) drops as inhibitor concentration rises, indicating that the presence of studied derivatives can prevent CS from dissolving, and the level of inhibition is dependent the concentration and kind of derivatives used.
2. Because of an increase in the overvoltage of each cathodic and anodic process in the attendance of inhibitors, both cathodic and anodic polarization curves were blocked. This pattern suggests that hydrogen evolution is a process that is controlled by activation.
3. Tafel curves demonstrated that adding B & A derivatives to the corrosive solution did not significantly change the corrosion potential (E_{corr}) [20]. In 0.5 M H_2SO_4 solution, the examined inhibitors can thus be categorized as mixed type inhibitors.
4. "According to the parallel cathodic Tafel lines, the addition of inhibitors to the 0.5 M H_2SO_4 solution does not alter the hydrogen evolution mechanism or the reduction of H^+ ions at the CS surface, which mostly happens through a charge transfer mechanism [20].
5. According to %IE values represented in Table 6, the inhibiting properties of the studied inhibitors at highest concentrations 50x10^{-6} M can be given in the following order: derivative(B) > derivative (A) with %IE values 91.7 and 89.5, respectively. These results are in good agreement with the results obtained from EIS measurements.

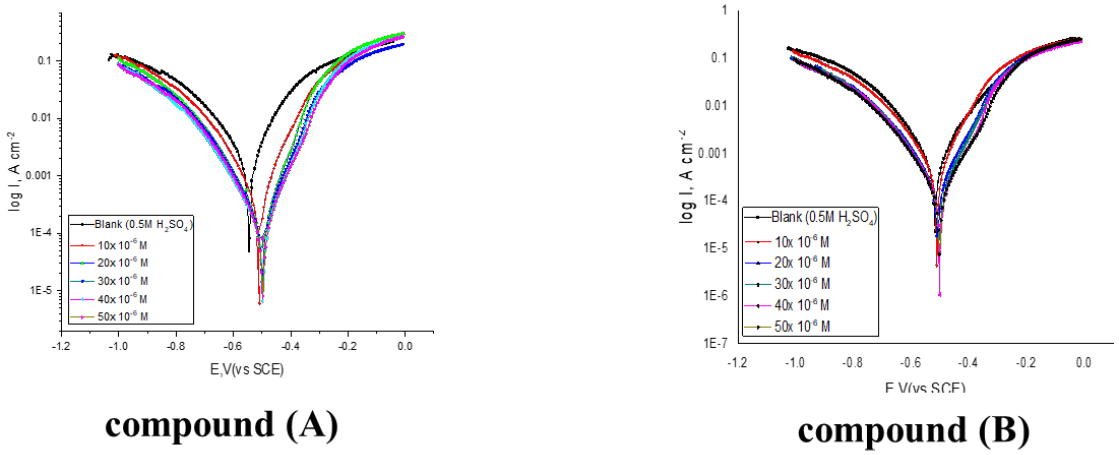

Fig 11. PP plots for CS with and without altered doses of compounds (A) and (B) at 25 °C

Table 6. Electrochemical parameters for CS in 0.5M H_2SO_4 with and absence of various doses of investigated derivatives

Comp.	Inh., Mx 10^6	E_{corr}, mV vs SCE	i_{corr}, μA cm^{-2}	$-\beta_c$, mV dec^{-1}	β_a, mV dec^{-1}	k_{corr}, mpy	Θ	%IE
Blank	**0.5 M H_2SO_4**	549±0.1453	756±0.1764	228.2±0.2027	71.90±0.1201	345.4	–	–
	10	541±0.1202	140±0.1732	124.9±0.2333	86.40±0.1453	64.01	0.815	81.5
	20	527±0.1527	115±0.1453	117.4±0.1764	54.60±0.2082	58.00	0.848	84.8
A	30	523±0.1202	111±0.0882	172.5±0.1202	87.00±0.1202	56.85	0.853	85.3
	40	521±0.0577	86.8±0.1453	103.4±0.1732	77.30±0.1155	46.00	0.885	88.5
	50	516±0.1764	78.9±0.2027	157.2±0.4484	87.60±0.1764	35.00	0.895	89.5
	10	549±0.1732	146±0.1453	187.1±0.1667	67.50±0.1453	64.70	0.806	80.6
	20	543±0.1453	123±0.1732	199.9±0.1154	64.70±0.1732	58.80	0.837	83.7
B	30	536±0.0882	102±0.0882	188.7±0.1764	60.70±0.0882	56.00	0.865	86.5
	40	516±0.1856	89.8±0.1202	199.5±0.1453	58.80±0.4372	46.46	0.881	88.1
	50	512±0.1764	62.4±0.2333	182.5±0.2309	43.70±0.2027	34.70	0.917	91.7

3.7 Quantum chemical calculations

To comprehend the characteristics and activity of the researched derivatives, a number of electronic parameters, like HOMO, LUMO and energy gap values were determined **(Figure 12).** HOMO and LUMO molecular orbital are calculated for all the structures using (PM3) method basis in the gas phase. HOMO is a symbol for the capacity for giving electron, whilst LUMO is a symbol for the capacity for receiving electron. The effectiveness of the inhibitor improved as the LUMO-HOMO energy gap shrank. A molecule's electrical dispersion is also measured by its dipole moment. The compound (B) has a better corrosion inhibition than compound (A), as shown in Table 7.

Table 7. The estimated quantum chemical properties for the tested derivatives

Compound	$-E_{HOMO}$	$-E_{LUMO}$	Dipole moment	ΔE
A	5.180	1.652	7.5332	3.528
B	5.480	2.082	9.1056	3.398

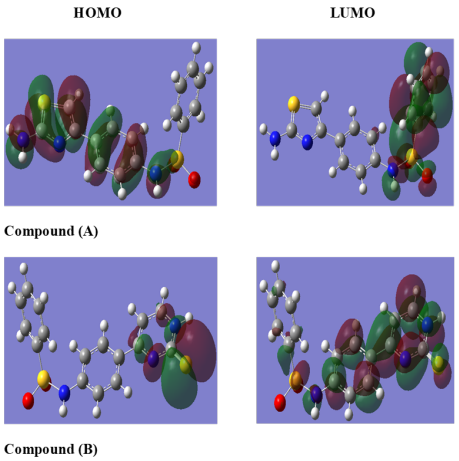

Fig 12. Quantum chemical of organic derivatives using PM3

3.8 Monte Carlo simulation

Monte Carlo simulation was utilized to find out more about the interactions between the molecules under study and the metal surface in an acidic and vacuum environment. Views of the more sturdy arrangement for the adsorption of the protonated and neutral varieties of sulfonamide derivatives on the surface of cleaved Fe (110) from the top and sides **(Figures 13 and 14)**. The parallel adsorption of the sulfonamide molecules ensures that the heteroatoms and π-electrons interface with the metallic surface of the Fe (110) in the best possible ways, enhancing the surface coverage. A higher concentration of inhibitor molecules in the test solution may cause more water molecules to be desorbed because the inhibitor molecules also remove water molecules from the adsorption sites. Adsorption energy, total energy, deformation energy, and stiff adsorption energy are the variables that were computed from the Monte Carlo simulation. The Table 8 clearly shows that sulfonamide derivative (B) has a higher adsorption energy than sulfonamide derivative (A) at the surface of Fe (110) in the presence of water, indicating that sulfonamide derivative (A) molecules have more durable adsorption on CS surface and form a robust adsorbed defensive layer, resulting in a corrosion shield for CS surface in damaging conditions, as demonstrated by both empirical and theoretical results.

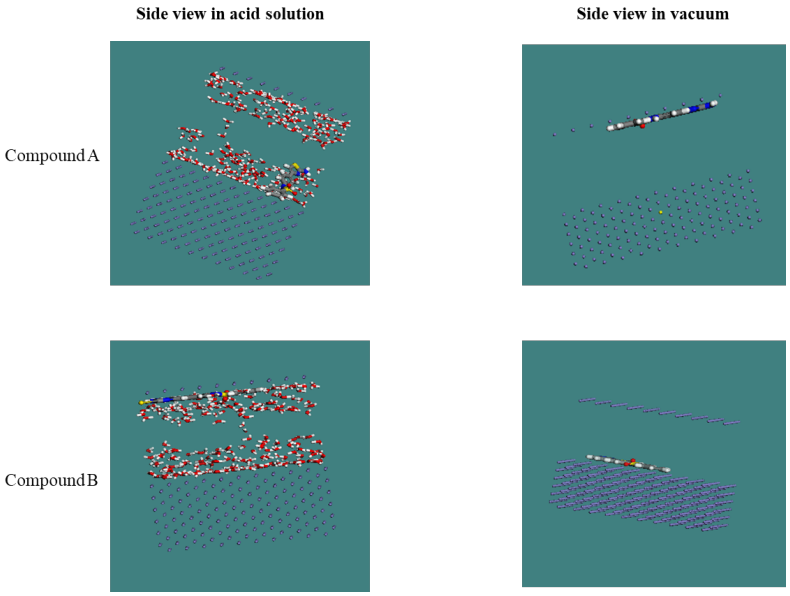

Fig 13. Side view for the most stable adsorption position of the inhibitors on Fe (110) surface in acid solution and vacuum

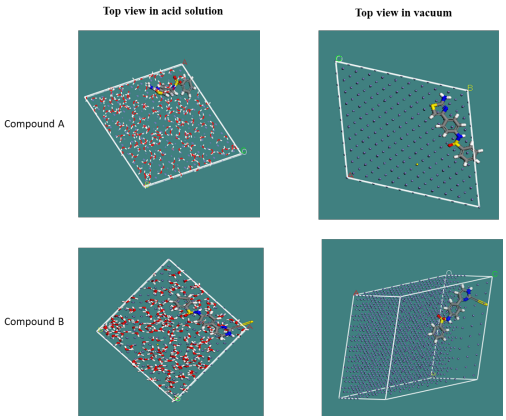

Fig 14. Top view for the most stable adsorption position of the inhibitors on Fe (110) surface in acid solution and vacuum

Table 8. Monte Carlo emulation variables computed for the more stable configuration of studied inhibitors on Fe (110) outer surface

Comp.	Total energy	Adsorption energy	Rigid adsorption energy	Deformation energy	Compound:d_{Ead}/d_{Ni}	H_2O:d_{Ead}/d_{Ni}
			Vacuum			
A	-138.487	-158.833	-165.381	6.548	-158.833	NA
B	-242.288	-170.700	-176.981	6.280	-170.700	NA
			Acid			
A	-3141.213	-8015.966	-3323.321	-4692.645	-84.871	-22.392
B	-3297.153	-8080.078	-3390.365	-4689.713	-216.803	-26.13

3.9 Surface morphology

3.9.1 ***FTIR technique***

FT-IR is a crucial analytical tool to understanding efficacious groups and characterizing bonding with metal [21]. Certain peaks of the IR spectra are corresponding to the function groups of the substances under investigation. After dipping in half molar H_2SO_4 + 50x10^{-6} M studied derivatives (A&B) for one day, the CS surface's spectra and those of derivatives A& B were attained and compared to each other **(Figure 15)**. The data of FT-IR showed that: the peaks of the function groups of the adsorbed chemicals show a tightly shifting, suggests that these substances have the potential to operate as corrosion inhibitors [21].

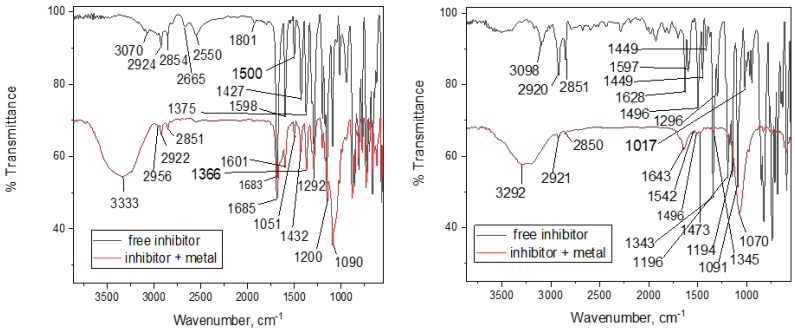

compound (A) **compound (B)**

Fig 15. FT-IR spectra of compounds (A) and (B)

3.9.2 *Scanning electron microscopy (SEM) studies*

"The image of CS before dispersion in acid solution shows the surface was smooth and without pits" (**Figure 16**). The photograph of CS after immersion in acid solution shows the surface was strongly attacked surrounded by corrosion products". "The photograph of CS after immersion in acid solution with the maximum" condensation of the inhibitors shows the surface of the CS becomes coated by cracked cover layer, compared with that of free acid and was free from pits and it became smooth (**Figure 16**). This demonstrates that the studied derivatives are adsorbed on the CS surface, generating a thick protective coating that impedes corrosion.

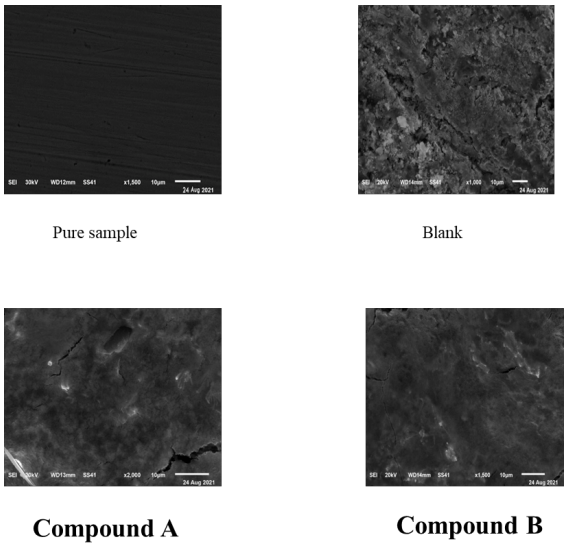

Fig 16. SEM micrographs for CS in 0.5M H_2SO_4 with and without the inhibitors

3.9.3 *Atomic force microscopy (AFM) analysis*

The RMS Roughness (S_q) and mean roughness (S_a), which are determined by mean lines and mean deviation from the mean, are calculated using the AFM test.Figure 17 shows the 3D surface of CS in the presence and absence of inhibitors. In the absence of the inhibitor with 0.5M H_2SO_4, the surface of CS is very rough (99.4 nm), whereas in the presence of the inhibitors with 0.5M H_2SO_4, there is less corrosion and less roughness (88.49 nm for compound A and 71.9 nm for compound B) because a film has formed on the surface CS surface.

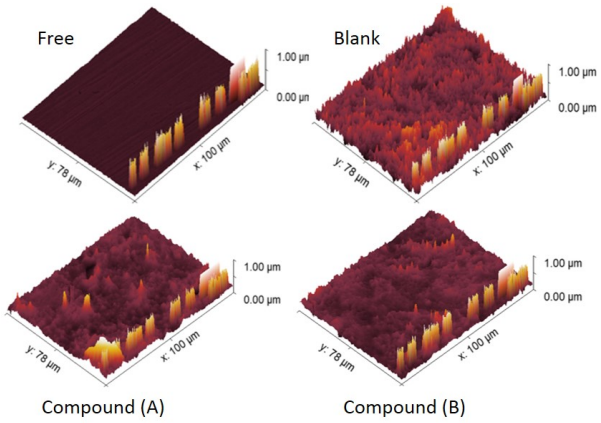

Fig 17. AFM micrographs for CS in 0.5M H_2SO_4 with and without the inhibitors

3.9.4 ***Energy dispersive X-ray spectroscopy (EDX) studies***

Figure 18 depicts the EDX spectra that demonstrate the specific peaks of certain elements constituting the CS in acidic medium without inhibitor. EDX spectra in the existence of the maximum dose of the chemicals display extra lines of carbon, nitrogen and oxygen owing to the layer of the adsorbed chemicals on CS. From Table 9, it was found that:

1. Intensities of C, O, S and N signal are enhanced and this due to N, C, S and O atoms present in the chemical composition of the inhibitors, indicating adsorption of the chemicals molecules on the surface of CS.
2. Fe peaks are suppressed in the existence of the inhibitors which is because of overlying inhibitor film.

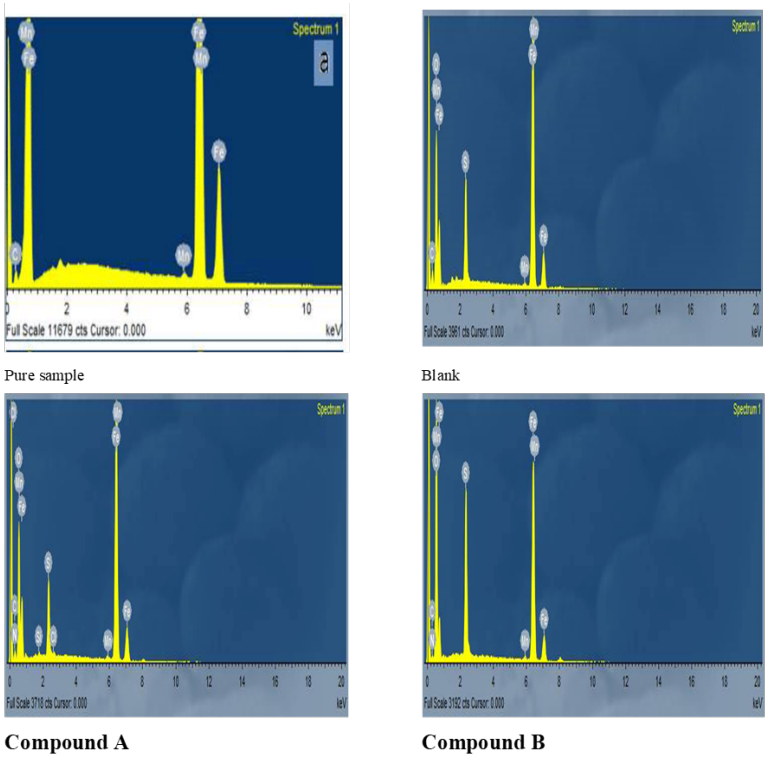

Fig 18. EDX spectra of CS with and without of 50 x 10^{-6} M of tested chemicals

Table 9. Surface characteristics (wt. %) of CS both earlier and later dispersion in half molar of sulfuric acid with and without of 50 x10^{-6} M of tested chemicals

(Mass %)	Fe	C	Mn	O	S	N
Free	95.77	3.54	0.90	–	–	–
Blank	80.29	2.97	0.81	15.5	0.43	–
Compound A	53.17	4.20	0.56	25.72	15.32	1.03
Compound B	52.06	7.60	0.62	24.21	14.26	1.25

3.10 Mechanism of corrosion inhibition

Adsorption can take four forms: i-Electrostatic attraction between the researched molecules and the CS. ii- Contact of unshared electron pairs in the analyzed derivatives with the CS. iii- Metal pi-electrons interaction vi- Summation of all the above. From the outcome data obtained from the various tests, corrosion hindrance of CS in half molar H_2SO_4 solutions by the investigated derivatives as designated from ML, PP, and EIS tests were depended on the nature of the inhibitor and the dose. These studied

compounds provide an adsorbed layer on the CS surface that blocks the attack of the corrosive medium on the surface, hence inhibiting the formation of active sites and reducing corrosion. Protonated inhibitor molecules (cationic) are physically attracted to the negatively charged surface of CS by electrostatic attraction once the SO_4^{2-} ions have adsorbed on it and turned it into such. IE is in the following order: B > A. The molecular size can be used to explain this arrangement of the IE of the tested substances; where B > A in molecular size. The utilized investigated chemicals as corrosion protection for CS in o.5M H_2SO_4 was deliberated according to physisorption on CS surface. This demonstrated by the data of ΔG^o_{ads} (less than 20 kJ mol^{-1}) also by temperature impact (%IE declines as temperature rises).

4 Conclusion

As a corrosion inhibitor, some benzene sulfonamides have been used to prevent corrosion of CS in a 0.5 M H2SO4 solution. It has been determined how well corrosion is inhibited using the weight reduction strategy. It is noted that 50 $x10^{-6}$ M of these inhibitors provide CS submerged in 0.5 M H_2SO_4 with more than 92% inhibitory effectiveness. Using electrochemical investigations such as polarization studies and AC impedance spectra, the mechanistic features of corrosion inhibition have been examined. The shift of the corrosion potential to values less than 85 mV(25 & 83.6 mV for A &B, respectively) in the presence of the inhibitor system during polarization research indicates that the inhibitors regulate the cathodic and the anodic reactions. The AC impedance spectra provide evidence that a protective coating has formed on the metal surface. This is supported by the fact that double layer capacitance has decreased and charge transfer resistance has increased. The inhibitor molecules adhere to the Langmuir adsorption isotherm during adsorption. The R^2 score is really high (0.999). FTIR spectra of the protective coating have been examined. SEM and AFM have been used to examine the protective film's surface morphology. It has been seen that the corroded metal's surface gets smoother when an inhibitor is present. The metal surface's Vickers hardness has been tested both before and after the experiment. It was shown that under the effect of corrosive medium, the surface becomes tougher in the presence of inhibitor than in the absence of inhibitor. Applications of the results in the petroleum sector are possible. In the CS pipelines, the inhibitor chemicals can be added with the water from a simulated oil well.

References

1) Adekunle AS, Olasunkanmi LO, Durodola SS, Oyekunle JAO, Olomola TO. Investigation on Corrosion Inhibition of Mild Steel by Extract of Dracaena arborea Leaves in Acidic Medium. *Chemistry Africa*. 2021;4:647–658. Available from: http://doi.org/10.1007/s42250-021-00246-8.
2) Ouakki M, Galai M, Cherkaoui M. Imidazole derivatives as efficient and potential class of corrosion inhibitors for metals and alloys in aqueous electrolytes: A review. *Journal of Molecular Liquids*. 2022;345. Available from: https://doi.org/10.1016/j.molliq.2021.117815.
3) Annon IA, Abbas AS, Al-Azzawi WK, Hanoon MM, Alamiery AA, Isahak WNRW, et al. Corrosion inhibition of mild steel in hydrochloric acid environment using thiadiazole derivative: Weight loss, thermodynamics, adsorption and computational investigations. *South African Journal of Chemical Engineering*. 2022;41:244–252. Available from: https://doi.org/10.1016/j.sajce.2022.06.011.
4) Kurtela M, Šimunović V, Stojanović I, Alar V. Effect of the cerium (III) chloride heptahydrate on the corrosion inhibition of aluminum alloy. *Materials and Corrosion*. 2020;71(1):125–147. Available from: https://doi.org/10.1002/maco.201911057.
5) Satyabama P, Rajendran S, Nguyen TA. Corrosion inhibition of aluminum by oxalate self-assembling monolayer. *Anti-Corrosion Methods and Materials*. 2019;66(6):768–773. Available from: https://doi.org/10.1108/ACMM-01-2019-2061.
6) Fouda AEAS, Etaiw SEH, Ismail MA, El-Aziz DMA, Eladl MM, M. Novel naphthybithiophene derivatives as corrosion inhibitors for carbon steel in 1 M HCl: Electrochemical, surface characterization and computational approaches. *Journal of Molecular Liquids*. 2022;367(Part A). Available from: https://doi.org/10.1016/j.molliq.2022.120394.
7) Mostfa MA, Gomaa H, Othman IMM, Ali GAM. Experimental and theoretical studies of a novel synthesized azopyrazole-benzenesulfonamide derivative as an efficient corrosion inhibitor for mild steel. *Journal of the Iranian Chemical Society*. 2021;18:1231–1241. Available from: https://doi.org/10.1007/s13738-020-02106-7.
8) Farag ZR, Moustapha ME, Anouar EH, El-Hafeez GMA. The inhibition tendencies of novel hydrazide derivatives on the corrosion behavior of mild steel in hydrochloric acid solution. *Journal of Materials Research and Technology*. 2022;16:1422–1434. Available from: https://doi.org/10.1016/j.jmrt.2021.12.035.
9) Alamiery AA. Anticorrosion effect of thiosemicarbazide derivative on mild steel in 1 M hydrochloric acid and 0.5 M sulfuric Acid: Gravimetrical and theoretical studies. *Materials Science for Energy Technologies*;4(2021):263–273. Available from: https://doi.org/10.1016/j.mset.2021.07.004.
10) Fouda AS, El-Dossoki FI, El-Hossiany A, Sello EA. Adsorption and Anticorrosion Behavior of Expired Meloxicam on Mild Steel in Hydrochloric Acid Solution. *Surface Engineering and Applied Electrochemistry*. 2020;56:491–500. Available from: https://doi.org/10.3103/S1068375520040055.
11) Tan B, Xiang B, Zhang S, Qiang Y, Xu L, Chen S, et al. Papaya leaves extract as a novel eco-friendly corrosion inhibitor for Cu in H2SO4 medium. *Journal of Colloid and Interface Science*. 2021;582(Part B):918–931. Available from: https://doi.org/10.1016/j.jcis.2020.08.093.
12) Saeed MT, Saleem M, Usmani S, Malik IA, Al-Shammari FA, Deen KM. Corrosion inhibition of mild steel in 1 M HCl by sweet melon peel extract. *Journal of King Saud University - Science*. 2019;31(4):1344–1351. Available from: https://doi.org/10.1016/j.jksus.2019.01.013.
13) Fouda AS, Abdel-Latif E, Helal HM, El-Hossiany A. Synthesis and Characterization of Some Novel Thiazole Derivatives and Their Applications as Corrosion Inhibitors for Zinc in 1 M Hydrochloric Acid Solution. *Russian Journal of Electrochemistry*. 2021;57:159–171. Available from: https://doi.org/10.1134/S1023193521020105.
14) Aslam J, Aslam R, Lone IH, Radwan NRE, Mobin M, Aslam A, et al. Inhibitory effect of 2-Nitroacridone on corrosion of low carbon steel in 1 M HCl solution: An experimental and theoretical approach. *Journal of Materials Research and Technology*. 2020;9(3):4061–4075. Available from: https://doi.org/10.1016/j.jmrt.2020.02.033.

15) Uwiringiyimana E, Sylvester OP, Joseph IV, Adams FV. The effect of corrosion inhibitors on stainless steels and aluminium alloys: A review. *The effect of corrosion inhibitors on stainless steels and*. 2016;10(2):23–32. Available from: https://doi.org/10.5897/AJPAC2016.0676.
16) Fouda AS, El-Aal AA, Sliem M, Abdullah A. Caprylamidopropyl Betaine as a Highly Efficient eco-friendly Corrosion Inhibitor for API X120 Steel in 1 M H2SO4. *Egyptian Journal of Chemistry*. 2020;63(3):759–776. Available from: https://ejchem.journals.ekb.eg/article_39775.html.
17) Fouda AS, Ahmed RE, El-Hossiany A. Chemical, Electrochemical and Quantum Chemical Studies for Famotidine Drug as a Safe Corrosion Inhibitor for α-Brass in HCl Solution. *Protection of Metals and Physical Chemistry of Surfaces volume*. 2021;57:398–411. Available from: https://doi.org/10.1134/S207020512101010X.
18) Elgyar OA, Ouf AM, El-Hossiany A, Fouda AES. The Inhibition Action of Viscum Album Extract on the Corrosion of Carbon Steel in Hydrochloric Acid Solution. *Biointerface Research in Applied Chemistry*. 2021;11(6):14344–14358. Available from: https://doi.org/10.33263/BRIAC116.1434414358.
19) Fouda AES, El-Gharkawy ES, Ramadan H, El-Hossiany A. Corrosion Resistance of Mild Steel in Hydrochloric Acid Solutions by Clinopodium acinos as a Green Inhibitor. *Biointerface Research in Applied Chemistry*. 2021;11(2):9786–9803. Available from: https://doi.org/10.33263/BRIAC112.97869803.
20) Fouda AES, Etaiws SEH, Hassan GS. Chemical, electrochemical and surface studies of new metal-organic frameworks (MOF) as corrosion inhibitors for carbon steel in sulfuric acid environment. *Scientific Reports* . 2022;12:1–2. Available from: https://doi.org/10.1038/s41598-022-21190-8.
21) Fouda AS, Wahba AM, Eissa M. Aluminum corrosion prevention in 1.0 M HCl solution by cystosiera myrica extract: An experimental and biological study. *Journal of the Indian Chemical Society*. 2022;99(8). Available from: https://doi.org/10.1016/j.jics.2022.100619.